The Late Miocene Biogenic Bloom : A globally distributed but not an ubiquitous event

Quentin Pillot, Baptiste Suchéras-Marx, Anta-Clarisse Sarr, Clara T Bolton, Yannick Donnadieu

The Late Miocene Biogenic Bloom : A globally distributed but not an ubiquitous event

Pillot Q.[1], **Suchéras-Marx B.**[1], **Sarr A-C.**[1], **Bolton C. T.**[1]**and Donnadieu Y.**[1]

[1]CEREGE, Aix Marseille Univ, CNRS, IRD, INRAE, Coll. France, France.

Key Points:

- The Late Miocene Biogenic Bloom (LMBB) is expressed in sediment cores in various oceanographic settings.
- Almost 40% of the sites in the compilation show no expression of the LMBB signal.
- The origin of the LMBB could be a generalised increase in upwelling activity.

Corresponding author: Pillot Q., `pillot@cerege.fr`

Abstract

The Late Miocene Biogenic Bloom (LMBB) is a late Miocene to early Pliocene oceanographic event characterized by high accumulation rates of opal from diatoms and calcite from calcareous nannofossils and planktic foraminifera. This multi-million year event has been recognized in sediment cores from the Pacific, Atlantic and Indian Oceans. The numerous studies discussing the LMBB lead us to believe that this event is omnipresent in all oceans, although this hypothesis need to be tested. Moreover, the origin of this event is still widely discussed. In this study we aim to provide a comprehensive overview of the geographical and temporal aspects of the LMBB by compiling published ocean drilling (DSDP, ODP and IODP) records of sedimentation rates, $CaCO_3$ and opal and terrigenous accumulation rates that cover the late Miocene and early Pliocene interval. Our data compilation shows that traces of the LMBB are present in many different locations but in a very heterogeneous way, highlighting that the LMBB is not a pervasive event. The compilation in addition shows that the sites where the LMBB is recorded are mainly located in areas with a high productivity regime (i.e. upwelling systems). We suggest that the most likely hypothesis to explain the LMBB is a global increase in upwelling intensity due to an increase in wind strength or an increase in deep water formation, ramping up global thermohaline circulation.

1 Introduction

The late Miocene is marked by a major event recognized in deep-sea sediments called the Late Miocene Biogenic Bloom (LMBB). This event is characterized by high rates of opal accumulation from diatoms and radiolarians and high rates of calcite accumulation from calcareous nannofossils and planktonic foraminifera (e.g. Farrell et al., 1995; Dickens & Owen, 1999; Grant & Dickens, 2002; Diester-Haass et al., 2005; Lyle & Baldauf, 2015; Drury et al., 2021; Bolton et al., 2022). The LMBB event, first described by Farrell et al. (1995), has been recovered in multiple sites of the world ocean (Figure 1) but its timing is heterogeneous across the sites and its signature in the data record has been identified from a variety of different proxies. Farrell et al. (1995) define the LMBB based on an increase in biogenic deposits ($CaCO_3$, biogenic silica (opal), and nannofossils) between 6.7 and 4.5 million years ago (Ma) in the Eastern Equatorial Pacific Ocean, and interpret this increase to be related to increased biological productivity. The Eastern Equatorial Pacific region was also studied by Lyle and Baldauf (2015) who observed the LMBB between 8 and 4.5 Ma, marked by long periods of high opal and $CaCO_3$ deposition. Records from the same region, with better resolution and updated age models, were used by Lyle et al. (2019) to estimate the end of the event at about 4.4 Ma, at a time of major decrease in sedimentation rate. Outside of the East Equatorial Pacific, Grant and Dickens (2002) identified the LMBB event in the southwestern Pacific Ocean, where it takes the form of an increase in $CaCO_3$ mass accumulation between 9 and 3.8 Ma with a maximum around 5 Ma. L. Zhang et al. (2009) identified the LMBB in records from the South China Sea that exhibit increased mass accumulation of $CaCO_3$ and opal between 12 and 6 Ma. In the Atlantic Ocean, Diester-Haass et al. (2005) identified the LMBB in three different regions. In the North Atlantic, $CaCO_3$ mass accumulation rate (MAR) and benthic foraminiferal accumulation rates reached a maximum at 5 Ma. This maximum was observed earlier in records from the tropical ocean (around 6 Ma) and the South Atlantic Ocean (around 8.2 Ma). In the South Atlantic (ODP site 1264), Drury et al. (2021) studied the evolution of $CaCO_3$ MAR at orbital resolution. The onset of the LMBB is detected at 7.8 Ma and the end at 3.3 Ma with an optimum between 7 and 6.4 Ma. Records from lower productivity regions in the Atlantic and Indian Oceans have also been used to identify the LMBB (Hermoyian & Owen, 2001). By measuring the rate of mass accumulation of phosphorus, they found a signature of the LMBB with peak productivity around 4-5 Ma. In the Indian Ocean, an increase in productivity between 9 and 3.5 Ma was identified by Dickens and Owen (1999) which is reflected in an increase in $CaCO_3$

mass accumulation as well as the spatial expansion of the Oxygen Minimum Zone. Nevertheless, Lübbers et al. (2019) suggest a much earlier onset of the LMBB in the Indian Ocean at 11.2 Ma based on an increase in Log (Ba/Ti) associated with a change in sediment color from red to green.

This increase in biogenic sedimentation is coeval with significant changes in the global climate system. Although the land-sea distribution has been quasi-stable since the late Miocene, the configuration of several major seaways evolved during this period: the Central American Seaway underwent final closure (O'Dea et al., 2016), the Bering Seaway opened (Gladenkov & Gladenkov, 2004) and the Indonesian Seaway underwent progressive restriction (Kuhnt et al., 2004), all of which likely triggered major changes in oceanic circulation (e.g. Brierley & Fedorov, 2016). Alongside these paleogeographic changes, global cooling occurred at the end of the Miocene, associated with an increase in the meridional sea surface temperature gradient (Herbert et al., 2016; Martinot et al., 2022). The global decrease in temperature is probably driven by a significant drop in the partial pressure of CO_2 in the atmosphere (pCO_2) from about 600 ppm in the middle Miocene to about 400 ppm in the early Pliocene (e.g. Rae et al., 2021). The establishment of a small permanent ice on Greenland is also inferred during the late Miocene (Helland & Holmes, 1997; John & Krissek, 2002; Bierman et al., 2016). The expansion of deserts may also be contemporary with this period (Schuster et al., 2006; Z. Zhang et al., 2014), although recent data from the tropical Atlantic margin highlight that the Sahara desert already existed 11 Ma ago (Crocker et al., 2022). Vegetation on land also underwent significant changes with the rise to dominance of plants using C_4 photosynthesis at the detriment of plants using C_3 photosynthesis (Tauxe & Feakins, 2020; Cerling et al., 1997). Some of these changes have been suggested as possible triggering mechanisms for the LMBB.

Two hypotheses have been proposed to explain the origin of the LMBB. This event could result from (1) an increase in nutrient supply from the continents to the oceans (e.g. Gupta et al., 2004; Pisias et al., 1995; Hermoyian & Owen, 2001; Filippelli, 1997) or (2) a redistribution of nutrients in the ocean due to a reorganization of oceanic circulation (e.g. Farrell et al., 1995; Dickens & Owen, 1999; Pisias et al., 1995).

An increase in nutrient supply is usually attributed either to enhanced weathering or to a shift in vegetation cover. A late pulse of uplift in the Tibetan Plateau region during the late Miocene (C. Wang et al., 2014) responsible for intensification of the Indian monsoon could have been responsible for increased continental weathering (Filippelli, 1997; Yang et al., 2019; Holbourn et al., 2018; Clift et al., 2020). This hypothesis is supported by the global increase in Ca and Si fluxes to the ocean (Pisias et al., 1995). Hermoyian and Owen (2001) also suggest that the uplift of the Andes at 8 Ma caused orographic precipitation and increased sediment flux to the Atlantic Ocean (Curry et al., 1995). An increase in nutrient supply from the continents could also be explained by an intensification of trade winds at the end of the Miocene, linked to the increase in latitudinal temperature gradient and also to widespread continental aridification (Dobson et al., 2001; Hovan, 1995; Diester-Haass et al., 2006; Herbert et al., 2016). A further hypothesis also suggests that the global spread of C_4 plants in the late Miocene would have resulted in the input of siliceous phytoliths into the ocean reservoir and may have played a role in increasing productivity by reducing silica limitation (Cortese et al., 2004; Pound et al., 2012).

The alternative hypothesis is the redistribution of nutrients caused by changes in oceanic circulation. Based on microfossil and $\delta^{13}C$ studies, Berger et al. (1993) suggested that an amplification of North Atlantic Deep Water (NADW, Wright and Miller (1996)) brought more nutrients into the Pacific Ocean, although Farrell et al. (1995) rather suggest no temporal link between NADW evolution and the LMBB. The restriction of the Central American Seaway may have played a role in the redistribution of nutrients by changing oceanic circulation patterns (Pisias et al., 1995; Farrell et al., 1995). Diester-Haass et al. (2002) also suggest that a change in the vertical distribution of nutrients could

result from an intensification of the global ocean circulation forced by an intensification of trade winds or by an increase in latitudinal temperature gradient (caused by the global decrease in pCO_2 and the growth of polar ice sheets).

While the initiation of the LMBB has been widely discussed in the literature (e.g. Farrell et al., 1995; Diester-Haass et al., 2002, 2006; Dickens & Owen, 1999; Reghellin et al., 2022), the termination of the event has been the subject of only a limited number of studies. Farrell et al. (1995) observe a distinct and permanent shift in the location of the maximum opal MAR at 4.4 Ma synchronous with the end of the LMBB. The authors attribute this shift to the final closure of the Central American Seaway that prevented surface currents from exchanging between the Atlantic and Pacific Oceans. More recently, Karatsolis et al. (2022) link the end of the LMBB with a decrease in insolation due to a particular orbital configuration. This drop in insolation would have caused a reduction in hydrological cycle intensity and therefore a decrease in continental weathering and nutrient supply to the ocean.

Because most of the published work on the LMBB focuses on specific cores where the event is recorded, we know where the bloom is present but mostly ignore places where the event is potentially not expressed. A global overview of the event is therefore lacking. The objective of this study is to provide a comprehensive perspective of the temporal and geographical aspects of the LMBB to help better understand the causes of the event and its impact on the carbon cycle. To do so we systematically compiled all available/published paleoceanographic records (from Deep Sea Drilling Project (DSDP), Oceanic Drilling Program (ODP), Integrated Ocean Drilling Program (IODP) and International ocean Discovery Program (IODP)), that inform on sediment accumulation during the late Miocene to early Pliocene time period. This compilation contains records of sedimentation rates as well as accumulation rates of $CaCO_3$, opal, and terrigenous material and provides an thorough analysis of the spatial and temporal distribution of the LMBB. In contrast to Karatsolis et al. (2022) who choose to focus on high resolution records only, we here choose a less selective approach because even lower resolution datasets or datasets that show no signature of the LMBB can help us understand its origin.

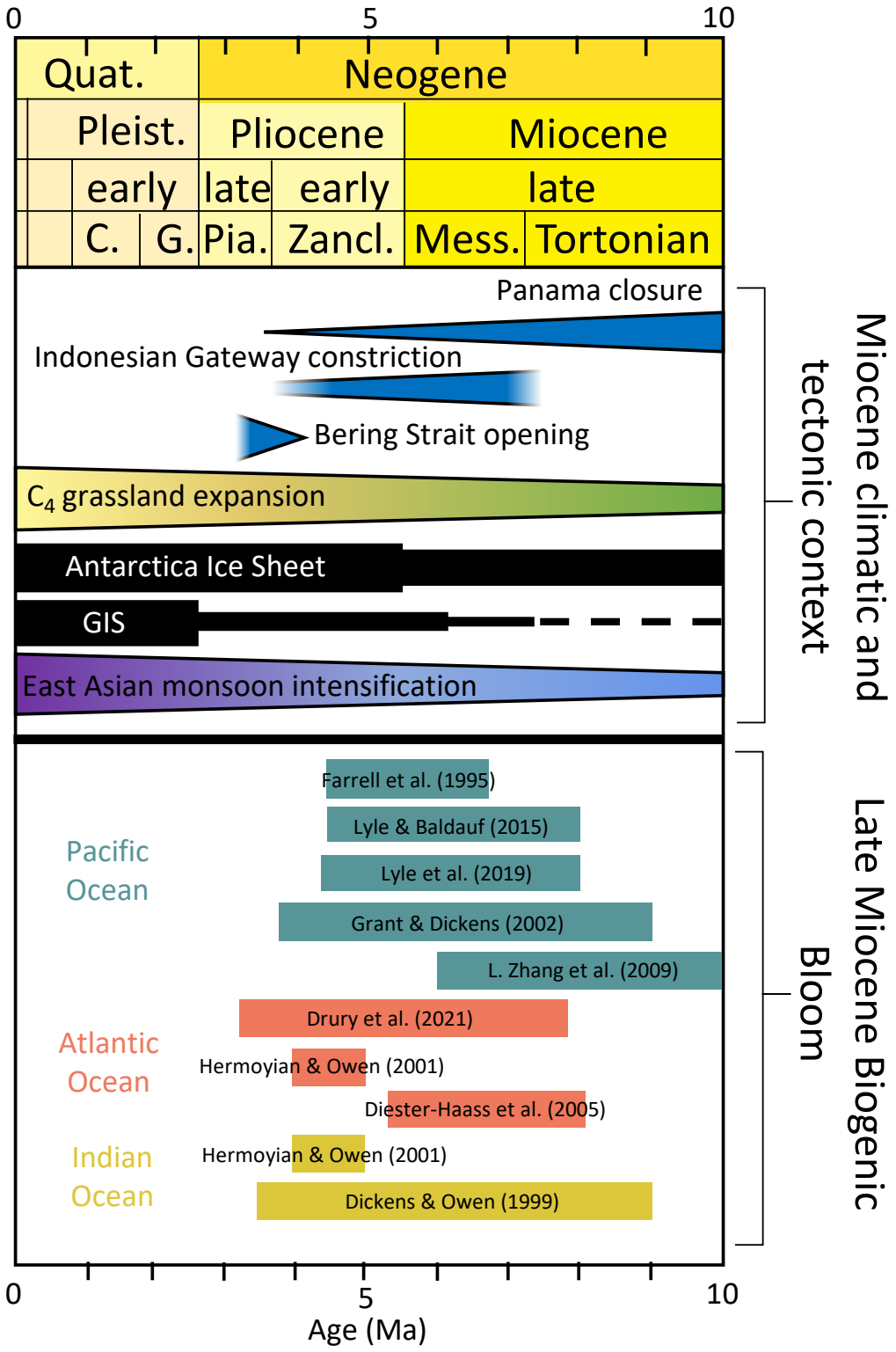

Figure 1. At the top, figure adapted from Steinthorsdottir et al. (2021). Climatic context (C_4 grassland expansion, Antartica and Greenland Ice sheet evoluion, East Asian monsoon intensification) and evolution of major seaways configuration during the late Miocene and Pliocene. GIS : Greenland Ice Sheet. Bottom, compilation of some publications related to the LMBB.

2 Methods

We compiled oceanographic data from DSDP, ODP and IODP expeditions that cover the late Miocene and early Pliocene. Data mining was performed by automatically collecting the Pangaea datasets that correspond to the selected time interval and that have at least one of the following variables: sedimentation rate, dry bulk density, mass accumulation rate (MAR), $CaCO_3$ accumulation rate, $bSiO_2$ accumulation rate (biogenic SiO_2) , $\%CaCO_3$, $\%bSiO_2$. The compilation was then improved by manually adding datasets absent from Pangaea but relevant to our study. The data compilation contains 155 datasets (122 are from Pangaea) from 118 different ocean drilling sites (Table 1). We consider here that within a single publication containing data from multiple sites, data from each site forms an individual dataset. There can therefore be several datasets per publication but also several datasets per site if several publications have studied the site in question.

Data processing was then carried out manually to remove datasets that were not relevant to the study, which include datasets that (1) do not provide any data between 9 and 3.5 Ma, (2) have a very coarse resolution (less than one data point per million years), or (3) show numerically unrealistic data (e.g. flat time series over a very long time period). The sites were additionally labeled to indicate whether they contained the LMBB signature, which is defined as an increase in carbonate or biogenic opal MAR or sedimentation rate between 9 and 3.5 Ma (which is the widest definition found in the literature, Dickens and Owen (1999)), with clearly identifiable increase and decrease phases. The results are split into four categories as follows : i) 'No', if the dataset shows no LMBB signature ; ii) 'Co', if the occurrence of the LMBB is controversial, that is, an increase in biogenic production can be identified but the timing is not consistent with the LMBB definition; iii) 'BB', if the LMBB is clearly identifiable; iv) "In", if there are not enough data before or after the interval of interest to robustly identify an increase ("In" standing for "inconclusive"). In the later case, we cannot conclude whether the LMBB is present in the dataset. In cases where there were several datasets for a single site, the label was assigned based on all the datasets considered together; if there was a contradiction between datasets, the dataset with the highest temporal resolution was chosen.

In order to perform a temporal comparison of the datasets, we also harmonized the geologic timescales used in all of the publications (Berggren et al., 1985, 1995; Gradstein et al., 2004, 2012, 2020; Palike et al., 2006) using the most recent one – Gradstein et al. (2020) – as a standard. This step was performed using the Neptune Sandbox Berlin database (Renaudie et al., 2020).

In addition, a geographical and temporal averaging system was implemented in order to plot time series. For a given oceanic basin (Pacific, Atlantic and Indian) and a given variable, all values of the corresponding datasets were grouped and segmented into 500 kyr bins to obtain a single time series. 500 kyr was chosen because many datasets – in particular Lyle (2003) – had a resolution of 500 kyr. Given that the resolution between different datasets is very heterogeneous, some datasets would have more weight in this average as they have more values in the bins. To avoid this bias, we therefore first averaged every dataset individually into 500 kyr bins before averaging them globally.

We then tried to identify potential oceanographic similarities between sites where the LMBB is present or absent. In order to do so, we computed the paleoproductivity at site locations using information from ocean biogeochemical simulations for the late Miocene (Sarr et al., 2022) that were performed with the IPSL-CM5A2 (Sepulchre et al., 2020) and PISCES-v2 (Aumont et al., 2015) models. To superimpose the position of the sites on the simulation outputs, we calculated the paleocoordinates of the sites for 10 Ma using the GPlates software (Qin et al., 2012) and the plate rotation model from Scotese (2016).

Table 1. Source of the data compilation. Sed rate : Sedimentation rate. Acc rate : Accumulation rate. MAR : Mass Accumulation Rate. DBD : Dry Bulk Density. A more detailed table can be found in the supplementary information.

Publication	Number of datasets	variables present in these data sets
Breza (1992)	1	Sed rate
Diester-Haass et al. (2004)	2	Acc rate $CaCO_3$
Diester-Haass et al. (2005)	3	Sed rate, Acc rate $CaCO_3$, $CaCO_3$, DBD
Diester-Haass et al. (2006)	4	Sed rate, MAR, Acc rate $CaCO_3$, $CaCO_3$
Drury et al. (2021)	1	Sed rate, $CaCO_3$, Acc rate $CaCO_3$, MAR, DBD
Dutkiewicz and Müller (2021)	16	Acc rate $CaCO_3$, DBD, $CaCO_3$, Sed rate
Farrell and Janecek (1991)	1	Sed rate, Acc rate $CaCO_3$, $CaCO_3$, DBD
Farrell et al. (1995)	11	Sed rate, Acc rate $CaCO_3$, $CaCO_3$, DBD
Gardner et al. (1986)	2	Sed rate, MAR, Acc rate $CaCO_3$, $CaCO_3$
Grant and Dickens (2002)	1	Acc rate $CaCO_3$, $CaCO_3$
Hayward et al. (2010)	1	Sed rate
Hermoyian and Owen (2001)	5	Sed rate, DBD
Janecek (1985)	2	Sed rate, MAR, DBD
Lyle et al. (1995)	11	Sed rate, Acc rate $CaCO_3$, $CaCO_3$
Lyle (2003)	57	Sed rate, MAR, Acc rate $CaCO_3$, $CaCO_3$, DBD
Lyle et al. (2019)	7	Sed rate, MAR, $CaCO_3$, DBD, $bSiO_2$
Müller et al. (1991)	1	Sed rate, MAR, Acc rate $CaCO_3$, DBD
Pälike et al. (2012)	4	Sed rate, MAR, $CaCO_3$, DBD, Acc rate $CaCO_3$
Peterson and Backman (1990)	3	MAR, Acc rate $CaCO_3$, $CaCO_3$
Si and Rosenthal (2019)	14	$CaCO_3$, MAR, Acc rate $CaCO_3$, Sed rate
Stax and Stein (1993)	4	MAR
Wagner (2002)	1	Sed rate, MAR
R. Wang et al. (2004)	1	Acc rate opal, $bSiO_2$
Winkler (1999)	1	Sed rate, MAR, Acc rate $CaCO_3$, $CaCO_3$
L. Zhang et al. (2009)	1	Sed rate, MAR, DBD

3 Results

3.1 Geographical analysis of the compilation

Among the 119 sites, the LMBB is present at 21 sites (Bb) while 33 other datasets remain controversial (Co). The LMBB is not present in 46 of the datasets (No) and its presence is inconclusive for 18 of the datasets (In). The LMBB is identified in both the Pacific, Atlantic and Indian Oceans (sites labeled "BB" and "Co", Figure 2). Most of the sites with a LMBB are localised at mid and low latitudes, suggesting that the LMBB is either absent or has not been recovered in the Southern or in the Arctic Oceans. The LMBB has been identified (certainly or controversially) in all the datasets from the northern part of the Indian Ocean. The presence of the LMBB in the Pacific and Atlantic Oceans is very heterogeneous. In some areas, sites with a LMBB and without a LMBB are very close geographically, such as in the Eastern Equatorial Pacific. The controversial sites have a more homogeneous distribution in terms of latitude.

The spatial distribution of sites where the LMBB has been clearly identified follows the same pattern as those where the presence of LMBB is controversial. There are only four sites that show a clear LMBB signature in the Atlantic basin, one in the Indian basin and all the remaining ones are located in the Pacific basin. Most of the LMBB sites are located in the low latitudes (between 30°S and 30°N, Figure 2a, 3a), except for ODP site 145-883 which is located in the northern Pacific.

In the Atlantic Ocean, areas where LMBB is clearly identifiable (off the American coastlines 5°N-40°E and off the African coastlines 30°S-4°W) are also areas where there are sites with no LMBB evidenced. Most of the isolated sites are sites without a LMBB and are located around the Mid-Atlantic Ridge. There is, however, a controversial presence of the LMBB at three isolated and open-ocean sites (ODP site 982B, ODP site 1088B and DSDP site 519).

In the Pacific Ocean, the LMBB signature is present off the coast of Australia, in the northern area of the Tasman Sea and also in the northern part of the Pacific Ocean. The LMBB is also mainly present in the eastern equatorial part although there are also many sites without the LMBB in this area. The Eastern Equatorial Pacific has a high concentration of sites with many of them showing the presence of the LMBB. Sites with a LMBB signature are mainly located between 5°N and 5°S while the sites without a LMBB are a few degrees further north and further south (except for DSDP site 572D).

In the Indian Ocean, the presence of the LMBB is in most cases controversial but one site clearly records it in the western tropical area, near the Seychelles archipelago (ODP site 707A). In the southern Indian Ocean the compilation has only two sites and they do not show any evidence of the LMBB. The remaining sites do not have enough data to conclude.

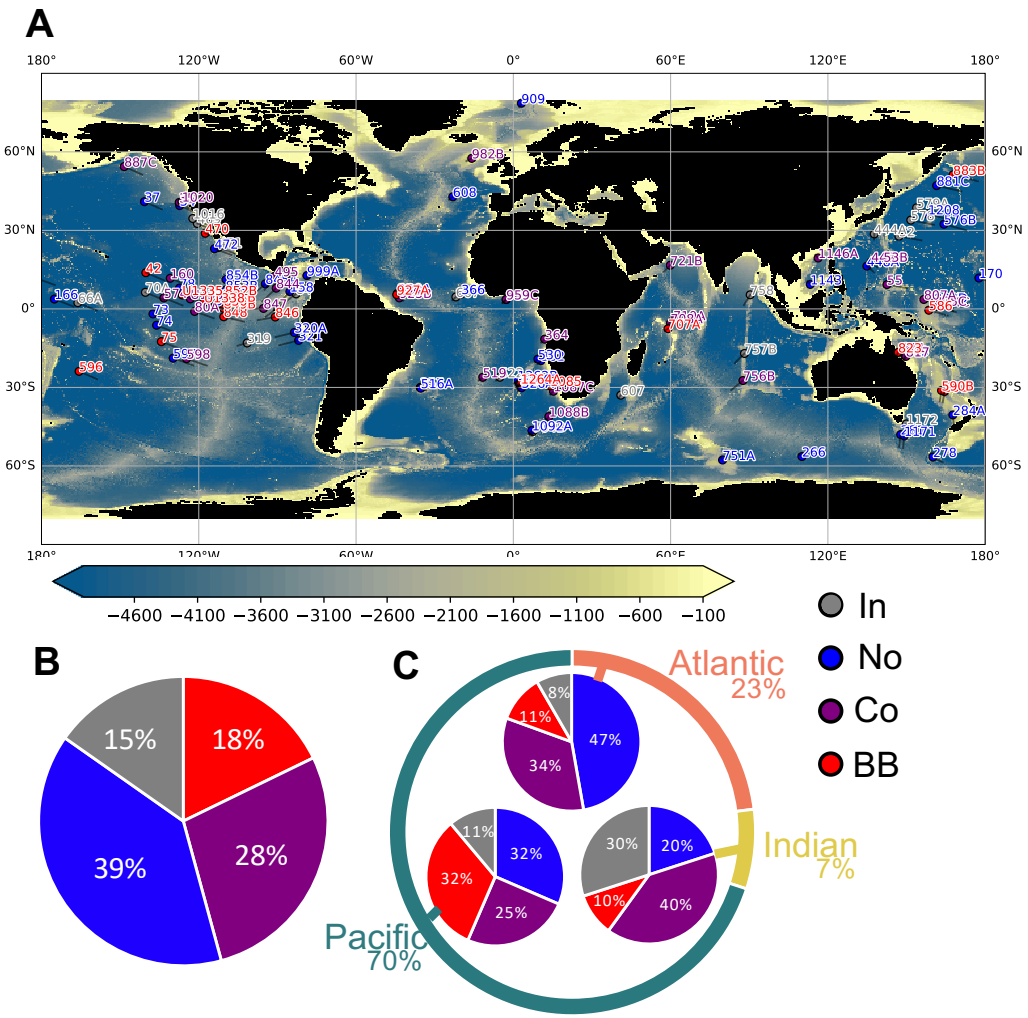

Figure 2. (A) Present-day bathymetry with dots showing the modern positions of the 118 labeled sites. The black line at the end of each point indicates the position of the site 10 million years ago. (B) Distribution of labels over the entire data compilation. (C) Distribution of the compilation for the three oceans.

3.2 Statistical analysis of compilation

The water depth of the sites where the LMBB is absent ranges between 1,000 and 5,000 metres with a large proportion of sites around 3,500 metres (Figure 3b). The depth of the sites where the LMBB is present is mainly between 1,500 and 4,000 metres. The average depth of sites where the LMBB is present (3,236 m) is almost equal to that of sites where the LMBB is absent (3,225 m). This suggests that the geographic distribution of sites where the LMBB is unambiguously identified is not biased by site depth thus by carbonate dissolution.

The simulated paleoproductivity at sites where a LMBB signature is visible is 0.66 $g/m^2/day$ on average (Figure 3d). Although most of the sites are located in areas of high simulated palaeoproductivity (> 0.7 $g/m^2/day$ - e.g. East Equatorial Pacific, Southeast Atlantic Ocean), the LMBB is also identified in some oligotrophic areas (< 0.3 $g/m^2/day$

- e.g. North Pacific, South Pacific Gyre, Figure S2). For sites where the LMBB is absent, the average simulated palaeoproductivity is 0.48 g/m^2/day. However, two groups can be distinguished, one around 0.25 g/m^2/day and one around 0.75 g/m^2/day. A group around 0.75 g/m^2/day also emerged in controversial sites.

If we consider instead the present-day productivity at sites, which is computed from average chlorophyll mass concentration values in seawater (from remote-sensing data of AquaMODIS satellite NASA Goddard Space Flight Center (2022)), the average value is almost identical for sites with and without the LMBB (around 0.20 mg/m^3, Figure 3e). There is significant variability for sites where the LMBB is absent or controversial, but for sites where the LMBB is not present, the values are centered around 0.18 mg/m^3.

To estimate the possible impact of continental nutrient inputs, the distance between each site and the nearest coastline was calculated (Figure 3f). On average the distance is higher for the sites where the LMBB is present (914 km) than for the sites where it is absent (786 km). However, the distribution is much more homogeneous for sites with the LMBB, while three groups of sites can be distinguished for the other labels, one around 500 km, one around 1,300 km and one around 2,000 km.

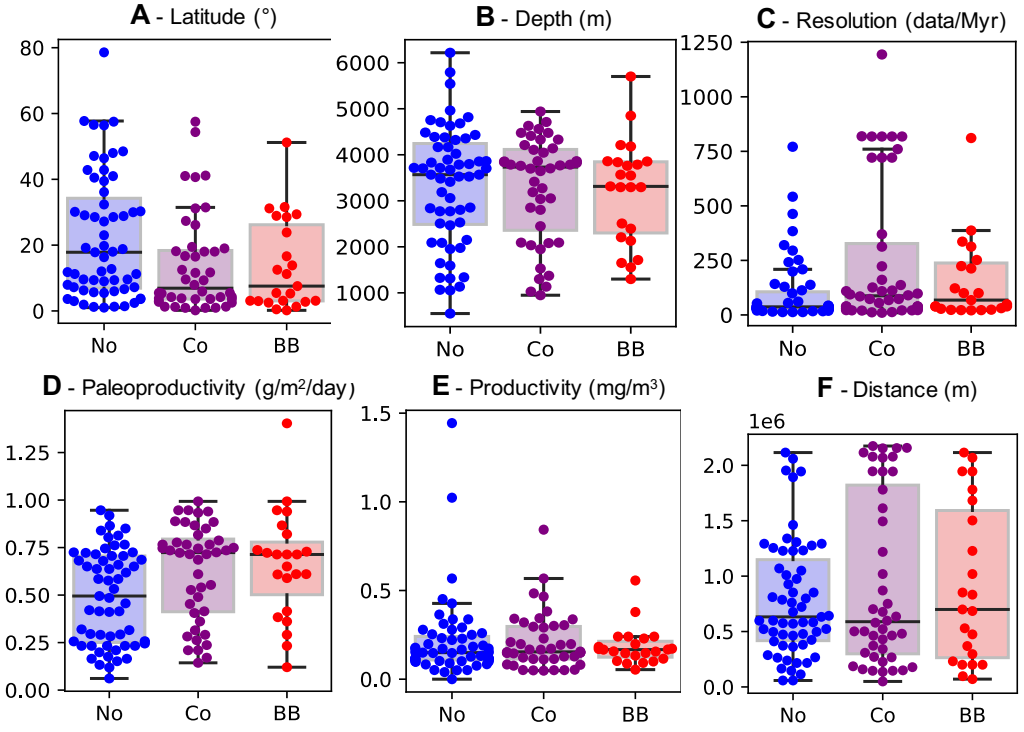

Figure 3. Box plot calculated for each label (each point represents a site). "No" - No LMBB ; "Co" - Controversial LMBB ; "BB" - LMBB is present. A: Average of absolute modern latitude values in degrees. B: Average depth of sites in metres. C: Average dataset resolution in number of data per million years. The site from Drury et al. (2021) is not shown because it is out of range (24,800 data/Myr). D : Average of the primary paleoproductivity value by phytoplankton from a late-Miocene simulation in g/m^2/day (from Sarr et al., 2022). E: Average chlorophyll mass concentration value in seawater in mg/m^3 (from remote-sensing data of AquaMODIS satellite NASA Goddard Space Flight Center (2022)). F: Average of the distances between the coordinates of the sites and the nearest coast (m).

3.3 Temporal analysis of the compilation

We also looked at the synchronicity of the event between different oceanic basins using time series that we computed following the procedure described in the Methods section (Figure 4). The values indicated hereafter are those of the unweighted average, meaning that datasets with better resolution have a higher weighting in the average. In the Atlantic Ocean, the signal was constructed from 12 different datasets, with a maximum of 1,639 data and a minimum of 153 in one bin. On this timeserie, $CaCO_3$ accumulation rate increases since 15 Ma with a strong increase around 7.5 Ma (+15.3 $g/m^2/y$). The maximum is reached around 7 Ma (34.1 $g/m^2/y$) and then there is a decrease that starts around 6.5 Ma and ends around 2 Ma. In the Indian Ocean, the signal was constructed from 4 different datasets, with a maximum of 51 data and a minimum of 2 in a bin. There is an increase around 7.5 Ma (+10 $g/m^2/y$) with a maximum around 7 Ma (20.5 $g/m^2/y$) then a decrease around 5.5 Ma. In the Pacific Ocean, the signal was constructed from 46 datasets, with a maximum of 620 data and a minimum of 45 in one bin. There is an increase in the rate of $CaCO_3$ accumulation from 10 Ma with a more abrupt increase around 7.5 Ma (+31.4 $g/m^2/y$). The maximum is around 7 Ma (44.5 $g/m^2/y$) with a decrease until 2 Ma.The comparison shows that the phase of increasing $CaCO_3$ accumulation rate around 7.5 Ma is synchronous between the three oceanic basins. The synchronicity of the end of the event is less distinct, with the decrease in biogenic sediment accumulation being more abrupt in the Pacific Ocean than in the Atlantic and Indian Oceans.

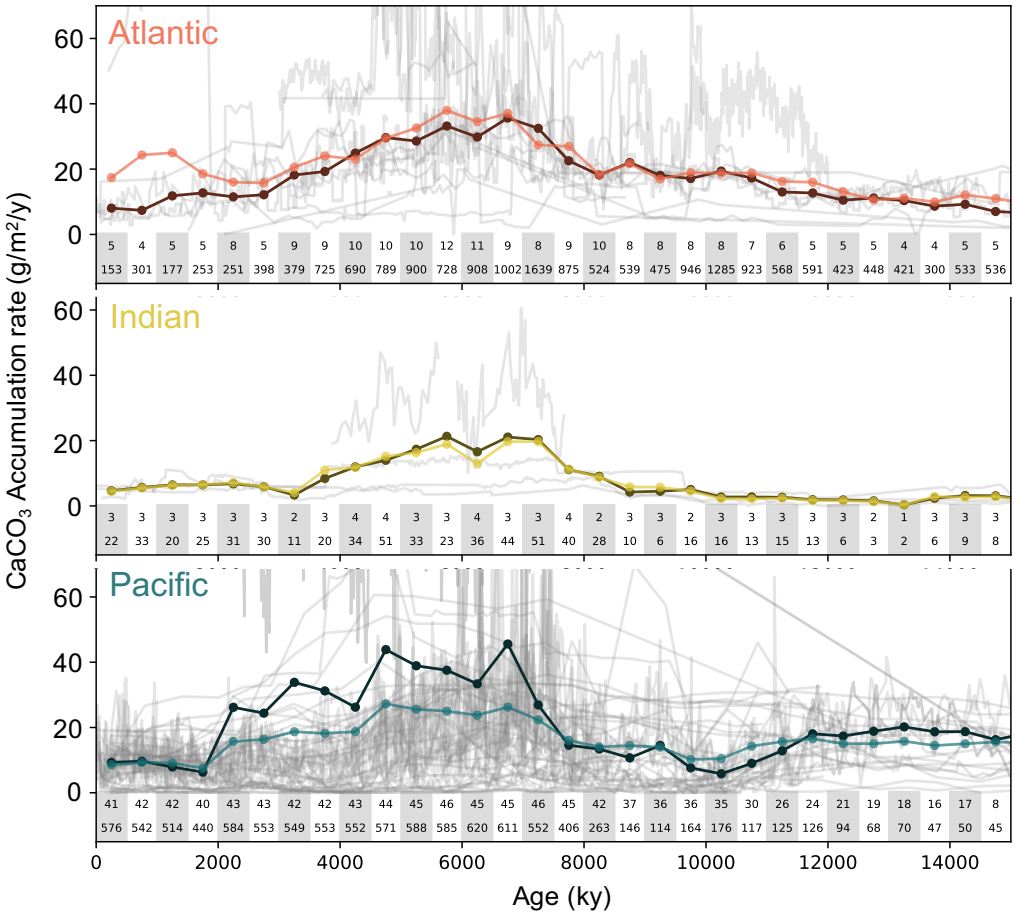

Figure 4. $CaCO_3$ accumulation rate from "BB" and "Co" labeled datasets for the three oceanic basins. Red, yellow and blue lines represent average weighted values to make each dataset equal (light colour) and unweighted average (dark colour) respectively, for each basin. The light grey lines represent the raw data used to calculate the average. Below each graph, we show the number of datasets used to calculate the average for each 500 kyr time bin (top line), and the number of data averaged (bottom line). The same figure with only the "BB" labeled sites can be found in supplementary Figure S1.

4 Discussion

4.1 Compilation biases and limitations

Several biases need to be highlighted to evaluate the limitations of this compilation before discussing its contribution to the mechanistic understanding of the LMBB. In order to label the datasets, it was necessary to establish criteria that defined the LMBB. These criteria – stated in the methods section – are based on the literature but are not necessarily shared by all authors, which makes it difficult to quantitatively and unequivocally identify the LMBB. Early studies defined the event in a specific region depending on local parameters and a bias may come from applying this definition globally. Indeed, the compilation showed that there was significant heterogeneity between datasets, which makes it difficult to apply a "global" definition. Observational biases are also present because the labeling of datasets relied on manual classification, as an automatic evalu-

ation was very complicated due to the definition bias exposed previously. The "Co" label was created for this purpose ; in order to classify all datasets that showed potential traces of LMBB but that could be classified as "BB" or "No" depending on the person performing the evaluation.

An important bias may come from the sampling of the data compilation. Indeed, a non-negligible proportion of the datasets comes from studies focusing specifically on the LMBB, which therefore published data where the LMBB signature was visible. There is a potential bias of publication of data from this time interval restricted toward those showing a clear LMBB record, thereby artificially increasing the number of sites with a LMBB signature in the compilation. In addition, the spatial distribution of sites included in the compilation is very heterogeneous. The majority of the compilation constitutes datasets from sites located in the Pacific Ocean (70%), while only 23% of the sites are located in the Atlantic Ocean and 7% in the Indian Ocean (Figure 2c). Very few sites are located at high latitudes (above 50°N and 50°S), or in the gyres of the South and North Pacific and of the North Atlantic oceans. This results in a geographically biased view of the LMBB as we lack information on the large-scale extension of the event. There is also temporal heterogeneity, as not all datasets cover exactly the same time interval, indeed many do not cover the entire LMBB time interval. This heterogeneity may prevent a proper temporal analysis of the compilation. Finally, some datasets come from studies with an orbital resolution and astronomical timescale (Drury et al., 2021) while others have only a few data points for a time window of several millions of years (Lyle, 2003). However, this resolution heterogeneity does not seem to impact labeling (Figure 3c) : sites with an identified LMBB do not have a better resolution than the sites without a LMBB. These potential biases must be kept in mind when interpreting the data compilation.

4.2 Does the compilation provide support for any of the LMBB hypotheses proposed in the literature ?

Despite the potential biases discussed above, our compilation has a worldwide coverage which opens the discussion on the origin of the LMBB. The compilation shows that the LMBB is a globally distributed but not ubiquitous event. Two hypotheses have been suggested in the literature in order to explain the existence of the event: (1) a global increase in the supply of nutrients to ocean basins through changes in continental weathering (Filippelli, 1997) or (2) a major redistribution of nutrients in the oceans (Farrell et al., 1995).

The spatial heterogeneity of the LMBB in the data compilation could be an element that supports the scenario of a change in nutrient supply from the continents. If this hypothesis is correct, it would seem logical that the LMBB signal would be visible at some sites (close to nutrient input from the continents) and not at others (isolated from these inputs) or at least reducing with the increased distance from the source and without a specific local to regional effect of transfer from oceanic currents or winds. However, the compilation of data also showed the global nature of this event and a "local" cause such as the Himalayan uplift cannot produce a rise in productivity on a global scale without redistribution, or if it did, it would have been homogeneous for areas at a great distance from the source (i. e. in the Atlantic Ocean). Furthermore, sites in the data compilation that are located in the South China Sea (ODP sites 1143 and 1146), thus directly affected by the East Asian monsoon system, do not show a clear LMBB signal. Calculations of the distances of the sites from the nearest coastline show that the LMBB is not present in areas particularly close to the coastline compared to areas where the LMBB appears to be absent, which partly contradicts this scenario. Nevertheless, it is important to consider that there can be local changes in the location of inputs that affect a particular site. For example, proximity of river outlet that changes its flow over time or shifting rainfall patterns. There is also evidence of micronutrient supply by dust

fluxes which, due to wind, can be transported a long distance from their source (Hovan, 1995; Diester-Haass et al., 2006). This wind-driven dust supply is particularly important as it is related to the cooling and aridification of the late Miocene (Pound et al., 2012; Herbert et al., 2016). However, our data compilation cannot highlight an increase in dust flux during this time interval. Moreover, the nutrient input would be then restricted to areas downwind of the arid and desert regions which is not clearly the case in our records. Karatsolis et al. (2022) suggest an end of the LMBB at 4.6-4.4 Ma related to a decrease in insolation which in turn would have caused a reduction in hydrological cycle intensity and continental weathering. Our compilation shows a significant decline in carbonate-related productivity in the Pacific Ocean at this time, although it does not appear to correspond to the end of the LMBB. Moreover, there is no decline observed at this time in the Indian and Atlantic Oceans. Furthermore, the hypothesis of a particular orbital configuration as a trigger for the end of the LMBB is incompatible with our results because we show a slow and continuous decline of carbonate accumulation in the terminal part of the LMBB. This slow decrease started as soon as the maximum was reached, around 7-6.5 Ma. Eventually, the increase in nutrient supply hypothesis seems not corresponding to our geographic and stratigraphic record.

Regarding the nutrient redistribution hypothesis, the Eastern Equatorial Pacific is an interesting case study as it has been widely discussed in the LMBB literature (Farrell et al., 1995; Lyle et al., 2019; Reghellin et al., 2022). Our compilation shows that sites with a LMBB signature cluster between 6°N and 5°S and between 90°W and 127°W (Figure 5). The LMBB signature is present at eight sites (plus three controversial ones) and is absent at DSDP site 572. A closer look at the data for DSDP site 572 shows that there is a decrease in productivity from 10 Ma and then an increase from 5 Ma to a peak at 3.5 Ma. This site has not been labelled "BB" because instead of having an increase in productivity at the end of the Miocene there is a decrease and the peak is reached at the moment when the "LMBB period" is over. The presence of this site without a LMBB might either be due to an error (in the definition of the event or in the interpretation of the signal) or to a particular geographical reason that remains undetermined. Without considering DSDP site 572, we observe that the sites where the LMBB is present were much closer to the Equator 10 Ma ago, which suggests an influence of equatorial upwelling on the increase in productivity (Lyle et al., 2019). Reghellin et al. (2022) suggested that the equatorial upwelling band was less parallel to the equator during the event and had a reduced spatial extent. Moreover, upwelling in this area appears to be strongest between 6.5 and 4.5 Ma, based on alkenone analyses from ODP sites 806 and 850 (Y. G. Zhang et al., 2017). These observations, which are in agreement with the compilation, support the scenario of nutrient redistribution as a driver of the LMBB. This redistribution may be a consequence of the closure of the Central American Seaway, which would result in the intensification of upwelling in the Eastern Equatorial Pacific, strongly increasing the surface nutrient concentration and thus primary productivity (Schneider & Schmittner, 2006). The Southeast Atlantic Ocean (around 30°S and 10°E) has also been studied in the context of the LMBB (Diester-Haass et al., 2004; Drury et al., 2021). In this area, the link between the LMBB and upwelling is more difficult to discern. Generally, sites where the LMBB is present are areas where simulated paleoproductivity is high (>0.5 g/cm^2/day, Figure 5) with the exception of ODP site 1264 (which is nonetheless the site with the highest resolution), which is in an area of low productivity (<0.4 g/cm^2/day) closely surrounded by five sites with no LMBB recorded. It is interesting to note that these sites are on the Walvis Ridge and that ODP site 1264 is much shallower than ODP sites 1262, 1265 and 1266 hence sometimes dissolution locally impact the record of the LMBB. Sites without the LMBB are generally in areas of low simulated paleoproductivity with the exception of ODP site 530 and DSDP site 362 (for these sites, the hypothesis of redistribution remains open to discussion). The calculation of simulated palaeoproductivity for each site (Figure 3d) shows that on average, the LMBB signature is mostly recorded at sites located in areas of high productivity (upwelling areas for example). This is consistent with a scenario of intensification of ocean circulation which can change the

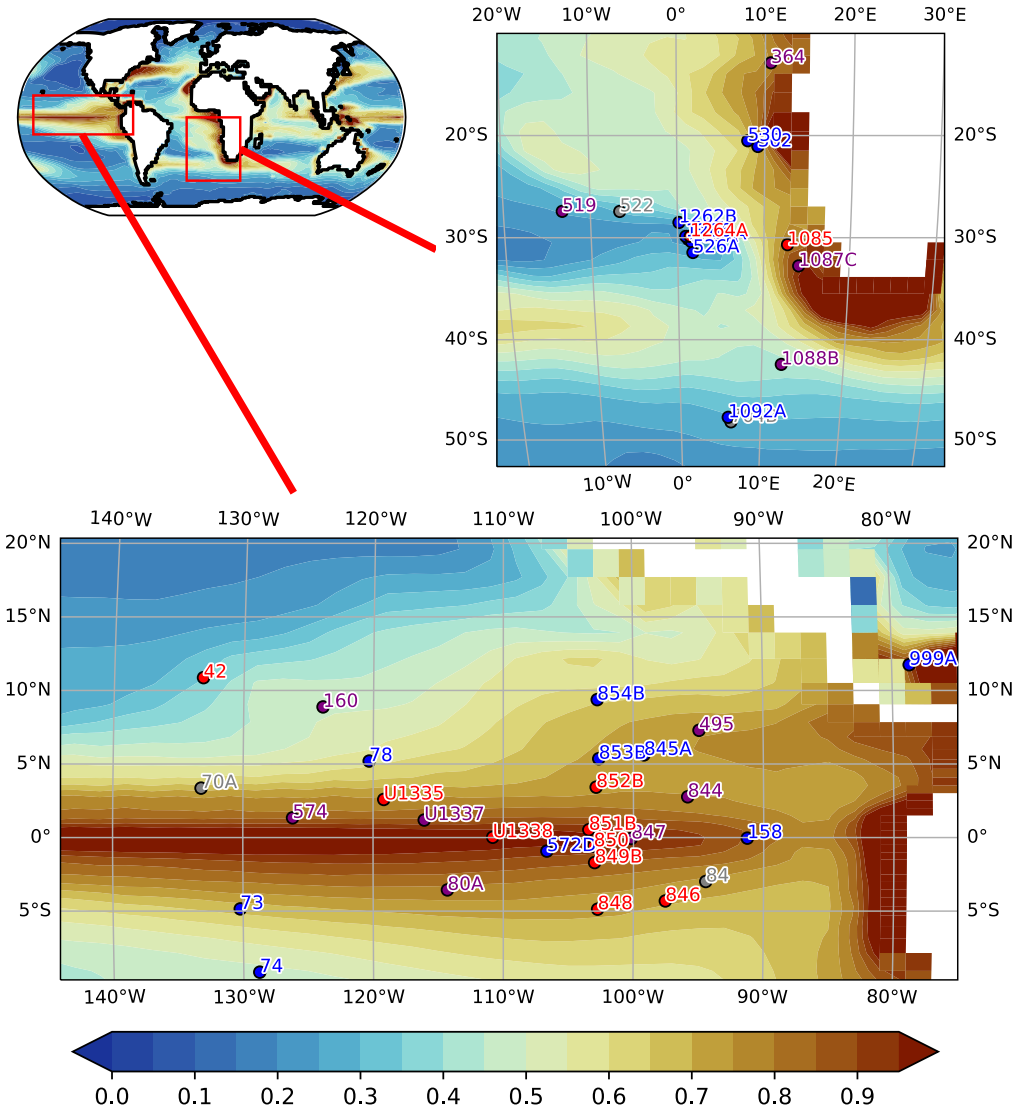

Figure 5. Primary productivity by phytoplankton in g/m^2/day for the late Miocene (simulation output from Sarr et al. (2022)) with dots showing the paleo-positions (10 Ma) of the labeled sites.

intensity of upwelling and induce a change in the vertical distribution of nutrients (Diester-Haass et al., 2002). Nutrient redistribution may also imply a transfer of nutrients from some geographic regions to others (Dickens & Owen, 1996). This would be consistent with the heterogeneous nature of LMBB in the data compilation. But according to this model, some sites should show a reverse signal, i.e. a decline in productivity between 9 and 3.5 Ma. Considering low influence of depth and dissolution on carbonate accumulation rates compiled (Figure 3b), no reverse signals are observed in the data compilation arguing against the redistribution hypothesis.

An alternative scenario would be to consider an increase in nutrients on a global scale without i) a redistribution with an increase of productivity in some regions compensated by a decrease elsewhere and ii) increase in continental inputs. This increase

in nutrients could come from the generalized intensification of upwelling systems. This intensification could have two origins, an intensification of the wind regime or an increase in deep water formation at high latitudes. The end of the Miocene is marked by a significant global cooling due to a decrease in the CO_2 level and a strengthening of the temperature gradient between the equator and the poles (Herbert et al., 2016; Martinot et al., 2022). The strengthening of this gradient leads to more air mass movement in the atmosphere and thus to an intensification of the Walker and Hadley cells (Kamae et al., 2011). Trade wind intensification is one consequence of this atmospheric reorganization, evidence of which has been observed in marine sediments (Hovan, 1995). The intensification of trade winds causes an increase in upwelling by Ekman pumping, especially in the equatorial Pacific (Bjerknes, 1969; Shankle et al., 2021) and results in increased productivity (Diester-Haass et al., 2006; Y. G. Zhang et al., 2017; Huguet et al., 2022). The late Miocene is also a period when the thermohaline circulation dominated by NADW and Antarctic Bottom Water became perennial (Poore et al., 2006). In general, NADW formation is thought to have intensified from the Miocene to the present day but its evolution is difficult to quantify (Poore et al., 2006). There are many factors that could have increased NADW production/strength in the late Miocene. For example, the decrease in CO_2 levels (Rae et al., 2021) in the late Miocene may have intensified NADW production (Bradshaw et al., 2015) as well as the transition from a mid-Miocene to present day geography (Herold et al., 2012). NADW may also be enhanced by the closure of the Central America Seaway (Nisancioglu et al., 2003; Schneider & Schmittner, 2006; Sepulchre et al., 2014), thought to have occurred during the Miocene (Montes et al., 2015). Bierman et al. (2016) showed that a small ice sheet might have existed on Greenland over the past 7.5 Ma. An ice sheet on Greenland can lead to an intensification of NADW, through atmospheric forcing (Pillot et al., 2022). Finally, NADW production also varied with the depth of the Greenland Scotland Ridge, which had phases of uplift and subsidence in the late Miocene (Wright & Miller, 1996; Poore et al., 2006; Hossain et al., 2020). Increased deep water formation results in the intensification of overturning cells (such as the AMOC) and therefore intensified upwelling systems. Following the same logic, a decrease in NADW production could have caused the end of the LMBB. The opening of the Bering Seaway in the early Pliocene (Gladenkov & Gladenkov, 2004), which according to modeling could have caused a weakening of the AMOC (Brierley & Fedorov, 2016), could potentially have been linked to the end of the LMBB.

4.3 Speculation on the link between the beginning of the LMBB and the Late Miocene Carbon Isotope Shift (LMCIS)

The new data compilation shows that there is a synchronicity between the onset of the LMBB and the LMCIS (Keigwin, 1979; Drury et al., 2017; Westerhold et al., 2020) for the three oceanic basins, a synchronicity that has already been discussed in the literature (Diester-Haass et al., 2005; Dickens & Owen, 1999; Grant & Dickens, 2002). This approximately 1‰ negative shift in benthic foraminiferal $\delta^{13}C$ extends from 7.5 to 6.7 Ma and corresponds to the last major carbon cycle change in Earth's history (Steinthorsdottir et al., 2021). The period of the $\delta^{13}C$ shift (7.5 to 6.7 Ma) corresponds to the most important phase of increasing productivity in the compilation and the productivity maximum (approx. 500,000 years, Figure 6). However, the isotopic shift lasts just under a million years and $\delta^{13}C$ never returns to its initial state, whereas the LMBB lasts several million years and biogenic sediment accumulation returns to a pre-event state. The causes of the LMCIS shift are still poorly understood. It may result from a global shift in $\delta^{13}C_{DIC}$ (Hodell et al., 2001; Bickert et al., 2004) caused by fractionation of organic matter in surface waters (Bickert et al., 2004) or a change in continental carbon flux (Du et al., 2022). This change may have been caused by the rapid expansion of C_4 plants between 8 and 6 Ma (Cerling et al., 1997), although this hypothesis appears to be temporally inconsistent (Drury et al., 2017; Tauxe & Feakins, 2020). The LMCIS may also have originated from a global high productivity event in the surface ocean (Grant & Dickens,

2002; Diester-Haass et al., 2005). The link between the LMBB and LMCIS supposes that the input of nutrients from the continents would produce a peak in dissolution and therefore a decrease in δ^{13}C values of dissolved inorganic carbon (Berger H, 1981; Diester-Haass et al., 2005; Bickert et al., 2004), yet this hypothesis is not consistent with our compilation, which shows no dissolution event. The LMCIS could also be a consequence of a change in global ocean circulation, in particular the contribution of NADW, which would result in a greater difference in δ^{13}C between deep waters from the north and those from the south (Hodell & Venz-Curtis, 2006; Butzin et al., 2011; Thomas & Via, 2007; Poore et al., 2006; Crichton et al., 2021). Considering the timing of the LMCIS (7.5 to 6.7 Ma), this hypothesis would support the NADW intensification scenario for the origin of the LMBB. In this case the LMCIS would not be a consequence of the LMBB but a parallel consequence of a common cause.

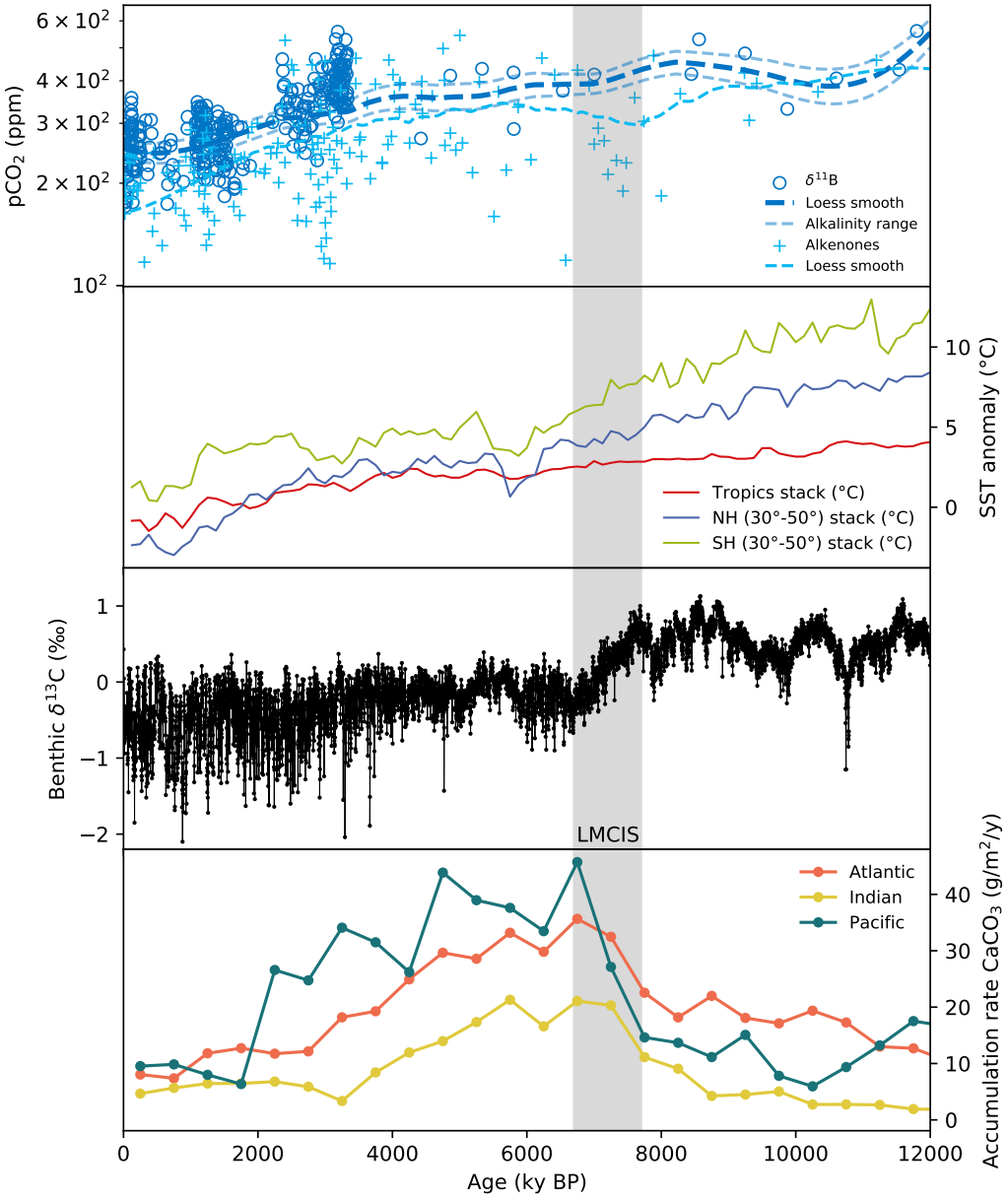

Figure 6. Top to bottom: Atmospheric pCO_2 reconstructions (ppm) from boron isotopes and alkenone $\delta^{13}C$ compiled in Rae et al. (2021). SST anomaly stacks for different latitudinal bands from Herbert et al. (2016). Megasplice benthic $\delta^{13}C$ evolution (‰) from Westerhold et al. (2020). $CaCO_3$ accumulation rate from "BB" and "Co" labeled datasets for the three ocean basins (Figure 4).

5 Conclusion

Our data compilation shows that traces of the LMBB are present at many different locations but in a very heterogeneous way. We therefore show that the LMBB is not a global event, as it is often considered in the literature to date, because its signature is absent from many sites. The compilation also shows that for the three oceanic basins, productivity shows a strong increase around 7.5 Ma, peaks around 7 Ma and then decreases until it reaches a pre-event state around 3.5 Ma. To explain the origin of the LMBB, the scenarios of increased nutrient input to the oceans and a redistribution of nutrients in the ocean cannot be ignored, although some aspects of our findings do not support these hypotheses. However, the compilation shows that the sites where the LMBB is recorded are mainly located in areas where there is a high productivity regime (i.e. upwelling systems). We propose that the most likely hypothesis to explain the LMBB is a global increase in upwelling intensity due to an increase in wind strength or an increase in deep water formation, ramping up global circulation. These increases may have been the result of major tectonic or climatic changes at the end of the Miocene, such as the closure of the Central American Seaway, the general decrease in temperature and CO_2 levels, subsidence of the Greenland-Scotland Ridge or the establishment of the Greenland ice-sheet. In future work, the forcing factors at the origin of the LMBB could be identified using a set of simulations from a coupled ocean/atmosphere models with late Miocene paleogeography and integrating a marine biogeochemistry module.

6 Open Research

All data used in this study have been previously published. The sources are available in Table 1 and in the Supplementary Table.

7 Author Contributions

Q. P. performed the data compilation and drafted the manuscript. The sites were labeled by Q. P. and B. S-M. All authors analyzed and discussed the results and contributed to the final version of the manuscript.

Acknowledgments

We are grateful to Johan Renaudie for his help in using Neptune Sandbox Berlin. We also thank Weimin Si for access to data and Jean-Baptiste Landant for discussions. We are also grateful to the French ANR project MioCarb (BSM,ANR-20-CE49-0002) for providing funding for this work.

References

Aumont, O., Ethé, C., Tagliabue, A., Bopp, L., & Gehlen, M. (2015, August). PISCES-v2: an ocean biogeochemical model for carbon and ecosystem studies. *Geoscientific Model Development*, *8*(8), 2465–2513. Retrieved 2022-01-03, from `https://gmd.copernicus.org/articles/8/2465/2015/` doi: 10.5194/gmd-8-2465-2015

Berger, W., Kroenke, L., Mayer, L., & et al. (Eds.). (1993, April). Proceedings of the Ocean Drilling Program, 130 Scientific Results. , *130*. Retrieved 2022-10-04, from `http://www-odp.tamu.edu/publications/130_SR/130TOC.HTM` doi: 10.2973/odp.proc.sr.130.1993

Berger H, V. E. (1981). Chemostratigraphy and Biostratigraphic Correlation: Exercises in Systematic Stratigraphy. Retrieved from `https://archimer.ifremer.fr/doc/00246/35689/` (Publication Title: Oceanologica Acta, Special issue Type: Article)

Berggren, W. A., Kent, D. V., Aubry, M.-P., & Hardenbol, J. (1995). Geochronology, time scales and global stratigraphic correlation.

Berggren, W. A., Kent, D. V., Flynn, J. J., & Van Couvering, J. A. (1985). Cenozoic geochronology. *Geological Society of America Bulletin*, *96*(11), 1407. Retrieved 2022-09-22, from https://pubs.geoscienceworld.org/gsabulletin/article/96/11/1407-1418/202998 doi: 10.1130/0016-7606(1985)96⟨1407:CG⟩2.0.CO;2

Bickert, T., Haug, G. H., & Tiedemann, R. (2004). Late Neogene benthic stable isotope record of Ocean Drilling Program Site 999: Implications for Caribbean paleoceanography, organic carbon burial, and the Messinian Salinity Crisis. *Paleoceanography*, *19*(1). Retrieved 2022-06-30, from http://onlinelibrary.wiley.com/doi/abs/10.1029/2002PA000799 (_eprint: https://agupubs.onlinelibrary.wiley.com/doi/pdf/10.1029/2002PA000799) doi: 10.1029/2002PA000799

Bierman, P. R., Shakun, J. D., Corbett, L. B., Zimmerman, S. R., & Rood, D. H. (2016, December). A persistent and dynamic East Greenland Ice Sheet over the past 7.5 million years. *Nature*, *540*(7632), 256–260. Retrieved 2020-08-28, from http://www.nature.com/articles/nature20147 doi: 10.1038/nature20147

Bjerknes, J. (1969, March). ATMOSPHERIC TELECONNECTIONS FROM THE EQUATORIAL PACIFIC. *Monthly Weather Review*, *97*(3), 163–172. Retrieved 2022-07-06, from https://journals.ametsoc.org/view/journals/mwre/97/3/1520-0493_1969_097_0163_atftep_2_3_co_2.xml (Publisher: American Meteorological Society Section: Monthly Weather Review) doi: 10.1175/1520-0493(1969)097⟨0163:ATFTEP⟩2.3.CO;2

Bolton, C. T., Gray, E., Kuhnt, W., Holbourn, A. E., Lübbers, J., Grant, K., ... Andersen, N. (2022, April). Secular and orbital-scale variability of equatorial Indian Ocean summer monsoon winds during the late Miocene. *Climate of the Past*, *18*(4), 713–738. Retrieved 2022-08-15, from https://cp.copernicus.org/articles/18/713/2022/ doi: 10.5194/cp-18-713-2022

Bradshaw, C. D., Lunt, D. J., Flecker, R., & Davies-Barnard, T. (2015, January). Disentangling the roles of late Miocene palaeogeography and vegetation – Implications for climate sensitivity. *Palaeogeography, Palaeoclimatology, Palaeoecology*, *417*, 17–34. Retrieved 2021-05-10, from https://linkinghub.elsevier.com/retrieve/pii/S0031018214004908 doi: 10.1016/j.palaeo.2014.10.003

Breza, J. (1992, April). High-resolution study of neogene ice-rafted debris, site 751, southern kerguelen plateau. , *120*. Retrieved from http://www-odp.tamu.edu/publications/120_SR/120TOC.HTM doi: 10.2973/odp.proc.sr.120.1992

Brierley, C. M., & Fedorov, A. V. (2016, June). Comparing the impacts of Miocene–Pliocene changes in inter-ocean gateways on climate: Central American Seaway, Bering Strait, and Indonesia. *Earth and Planetary Science Letters*, *444*, 116–130. Retrieved 2021-05-10, from https://linkinghub.elsevier.com/retrieve/pii/S0012821X16300978 doi: 10.1016/j.epsl.2016.03.010

Butzin, M., Lohmann, G., & Bickert, T. (2011, February). Miocene ocean circulation inferred from marine carbon cycle modeling combined with benthic isotope records. *Paleoceanography*, *26*(1), PA1203. Retrieved 2021-05-10, from http://doi.wiley.com/10.1029/2009PA001901 doi: 10.1029/2009PA001901

Cerling, T. E., Harris, J. M., MacFadden, B. J., Leakey, M. G., Quade, J., Eisenmann, V., & Ehleringer, J. R. (1997, September). Global vegetation change through the Miocene/Pliocene boundary. *Nature*, *389*(6647), 153–158. Retrieved 2022-09-22, from http://www.nature.com/articles/38229 doi: 10.1038/38229

Clift, P. D., Kulhanek, D. K., Zhou, P., Bowen, M. G., Vincent, S. M., Lyle, M., & Hahn, A. (2020). Chemical weathering and erosion responses to changing monsoon climate in the late miocene of southwest asia. *Geological Magazine*, *157*(6), 939–955.

Cortese, G., Gersonde, R., Hillenbrand, C.-D., & Kuhn, G. (2004, August). Opal sedimentation shifts in the World Ocean over the last 15 Myr. *Earth and Planetary Science Letters*, *224*(3-4), 509–527. Retrieved 2020-11-09, from https://linkinghub.elsevier.com/retrieve/pii/S0012821X04003553 doi: 10.1016/j.epsl.2004.05.035

Crichton, K. A., Ridgwell, A., Lunt, D. J., Farnsworth, A., & Pearson, P. N. (2021, October). Data-constrained assessment of ocean circulation changes since the middle Miocene in an Earth system model. *Climate of the Past*, *17*(5), 2223–2254. Retrieved 2022-10-04, from https://cp.copernicus.org/articles/17/2223/2021/ doi: 10.5194/cp-17-2223-2021

Crocker, A. J., Naafs, B. D. A., Westerhold, T., James, R. H., Cooper, M. J., Röhl, U., ... Wilson, P. A. (2022, July). Astronomically controlled aridity in the Sahara since at least 11 million years ago. *Nature Geoscience*. Retrieved 2022-07-26, from https://www.nature.com/articles/s41561-022-00990-7 doi: 10.1038/s41561-022-00990-7

Curry, W., Shackleton, N., Richter, C., Backman, J., Bassinot, F., Bickert, T., ... others (1995). Leg synthesis. *Proceedings Ocean Drilling Program, Initial Reports 155*, 17–21. (Publisher: Ocean Drilling Program)

Dickens, G. R., & Owen, R. M. (1996, April). Sediment geochemical evidence for an early-middle Gilbert (early Pliocene) productivity peak in the North Pacific Red Clay Province. *Marine Micropaleontology*, *27*(1-4), 107–120. Retrieved 2020-11-09, from https://linkinghub.elsevier.com/retrieve/pii/0377839895000542 doi: 10.1016/0377-8398(95)00054-2

Dickens, G. R., & Owen, R. M. (1999, September). The Latest Miocene–Early Pliocene biogenic bloom: a revised Indian Ocean perspective. *Marine Geology*, *161*(1), 75–91. Retrieved 2020-11-09, from https://linkinghub.elsevier.com/retrieve/pii/S0025322799000572 doi: 10.1016/S0025-3227(99)00057-2

Diester-Haass, L., Billups, K., & Emeis, K. C. (2005). In search of the late Miocene–early Pliocene "biogenic bloom" in the Atlantic Ocean (Ocean Drilling Program Sites 982, 925, and 1088). *Paleoceanography*, *20*(4). Retrieved 2022-03-15, from http://onlinelibrary.wiley.com/doi/abs/10.1029/2005PA001139 (_eprint: https://agupubs.onlinelibrary.wiley.com/doi/pdf/10.1029/2005PA001139) doi: 10.1029/2005PA001139

Diester-Haass, L., Billups, K., & Emeis, K. C. (2006). Late Miocene carbon isotope records and marine biological productivity: Was there a (dusty) link? *Paleoceanography*, *21*(4). Retrieved 2022-03-15, from http://onlinelibrary.wiley.com/doi/abs/10.1029/2006PA001267 (_eprint: https://agupubs.onlinelibrary.wiley.com/doi/pdf/10.1029/2006PA001267) doi: 10.1029/2006PA001267

Diester-Haass, L., Meyers, P. A., & Bickert, T. (2004). Carbonate crash and biogenic bloom in the late Miocene: Evidence from ODP Sites 1085, 1086, and 1087 in the Cape Basin, southeast Atlantic Ocean. *Paleoceanography*, *19*(1). Retrieved 2022-03-15, from http://onlinelibrary.wiley.com/doi/abs/10.1029/2003PA000933 (_eprint: https://agupubs.onlinelibrary.wiley.com/doi/pdf/10.1029/2003PA000933) doi: 10.1029/2003PA000933

Diester-Haass, L., Meyers, P. A., & Vidal, L. (2002, February). The late Miocene onset of high productivity in the Benguela Current upwelling system as part of a global pattern. *Marine Geology*, *180*(1-4), 87–103. Retrieved

2020-11-09, from https://linkinghub.elsevier.com/retrieve/pii/S0025322701002079 doi: 10.1016/S0025-3227(01)00207-9

Dobson, D. M., Dickens, G. R., & Rea, D. K. (2001, January). Terrigenous sediment on Ceara Rise: a Cenozoic record of South American orogeny and erosion. *Palaeogeography, Palaeoclimatology, Palaeoecology*, *165*(3-4), 215–229. Retrieved 2022-09-22, from https://linkinghub.elsevier.com/retrieve/pii/S0031018200001619 doi: 10.1016/S0031-0182(00)00161-9

Drury, A. J., Liebrand, D., Westerhold, T., Beddow, H. M., Hodell, D. A., Rohlfs, N., ... Lourens, L. J. (2021, October). Climate, cryosphere and carbon cycle controls on Southeast Atlantic orbital-scale carbonate deposition since the Oligocene (30–0 Ma). *Climate of the Past*, *17*(5), 2091–2117. Retrieved 2022-03-03, from https://cp.copernicus.org/articles/17/2091/2021/ doi: 10.5194/cp-17-2091-2021

Drury, A. J., Westerhold, T., Frederichs, T., Tian, J., Wilkens, R., Channell, J. E., ... Röhl, U. (2017, October). Late Miocene climate and time scale reconciliation: Accurate orbital calibration from a deep-sea perspective. *Earth and Planetary Science Letters*, *475*, 254–266. Retrieved 2022-04-29, from https://linkinghub.elsevier.com/retrieve/pii/S0012821X17304223 doi: 10.1016/j.epsl.2017.07.038

Du, J., Tian, J., & Ma, W. (2022, April). The Late Miocene Carbon Isotope Shift driven by synergetic terrestrial processes: A box-model study. *Earth and Planetary Science Letters*, *584*, 117457. Retrieved 2022-07-06, from https://linkinghub.elsevier.com/retrieve/pii/S0012821X22000930 doi: 10.1016/j.epsl.2022.117457

Dutkiewicz, A., & Müller, R. D. (2021, July). The carbonate compensation depth in the South Atlantic Ocean since the Late Cretaceous. *Geology*, *49*(7), 873–878. Retrieved 2022-01-14, from https://pubs.geoscienceworld.org/geology/article/49/7/873/596162/The-carbonate-compensation-depth-in-the-South doi: 10.1130/G48404.1

Farrell, J. W., & Janecek, T. R. (1991, November). Late neogene paleoceanography and paleoclimatology of the northeast indian ocean (site 758). , *121*. Retrieved 2022-10-04, from http://www-odp.tamu.edu/publications/121_SR/121TOC.HTM doi: 10.2973/odp.proc.sr.121.1991

Farrell, J. W., Raffi, I., Janecek, T. R., Murray, D. W., Levitan, M., Dadey, K. A., ... Hovan, S. (1995). LATE NEOGENE SEDIMENTATION PATTERNS IN THE EASTERN EQUATORIAL PACIFIC OCEAN. , 40.

Filippelli, G. M. (1997). Intensification of the Asian monsoon and a chemical weathering event in the late Miocene–early Pliocene: Implications for late Neogene climate change. , 4.

Gardner, J. V., Dean, W. E., Bisagno, L., Hemphill, E., & Survey, U. G. (1986, January). Late neogene and quaternary coarse-fraction and carbonate stratigraphies for site 586 on ontong-java plateau and site 591 on lord howe rise. , *90*. Retrieved 2022-03-15, from http://deepseadrilling.org/90/dsdp_toc.htm doi: 10.2973/dsdp.proc.90.1986

Gladenkov, A. Y., & Gladenkov, Y. B. (2004). Onset of Connections between the Pacific and Arctic Oceans through the Bering Strait in the Neogene. , *12*(2), 13.

Gradstein, F. M., Ogg, J. G., Schmitz, M. D., Ogg, G. M., Agterberg, F. P., Anthonissen, D. E., ... Xiao, S. (2012). The Geologic Time Scale. In F. M. Gradstein, J. G. Ogg, M. D. Schmitz, & G. M. Ogg (Eds.), *The Geologic Time Scale* (pp. ix–xi). Boston: Elsevier. Retrieved from https://www.sciencedirect.com/science/article/pii/B9780444594259100034 doi: https://doi.org/10.1016/B978-0-444-59425-9.10003-4

Gradstein, F. M., Ogg, J. G., Schmitz, M. D., Ogg, G. M., Agterberg, F. P., Aretz, M., ... Vernyhorova, Y. (2020). Geologic Time Scale 2020. In

F. M. Gradstein, J. G. Ogg, M. D. Schmitz, & G. M. Ogg (Eds.), *Geologic Time Scale 2020* (pp. xi–xiv). Elsevier. Retrieved from https://www.sciencedirect.com/science/article/pii/B978012824360200036X doi: https://doi.org/10.1016/B978-0-12-824360-2.00036-X

Gradstein, F. M., Ogg, J. G., & Smith, A. G. (2004). *A Geologic Time Scale 2004, Cambridge Univ. Press; 589 pp.*

Grant, K. M., & Dickens, G. R. (2002). Coupled productivity and carbon isotope records in the southwest pacific ocean during the late miocene–early pliocene biogenic bloom. *Palaeogeography, Palaeoclimatology, Palaeoecology*, *187*(1-2), 61–82.

Gupta, A. K., Singh, R. K., Joseph, S., & Thomas, E. (2004). Indian Ocean high-productivity event (10–8 Ma): Linked to global cooling or to the initiation of the Indian monsoons? *Geology*, *32*(9), 753. Retrieved 2020-11-09, from https://pubs.geoscienceworld.org/geology/article/32/9/753-756/103705 doi: 10.1130/G20662.1

Hayward, B. W., Johnson, K., Sabaa, A. T., Kawagata, S., & Thomas, E. (2010, April). Cenozoic record of elongate, cylindrical, deep-sea benthic foraminifera in the North Atlantic and equatorial Pacific Oceans. *Marine Micropaleontology*, *74*(3-4), 75–95. Retrieved 2022-03-15, from https://linkinghub.elsevier.com/retrieve/pii/S0377839810000101 doi: 10.1016/j.marmicro.2010.01.001

Helland, P., & Holmes, M. (1997, December). Surface textural analysis of quartz sand grains from ODP Site 918 off the southeast coast of Greenland suggests glaciation of southern Greenland at 11 Ma. *Palaeogeography, Palaeoclimatology, Palaeoecology*, *135*(1-4), 109–121. Retrieved 2021-08-17, from https://linkinghub.elsevier.com/retrieve/pii/S0031018297000254 doi: 10.1016/S0031-0182(97)00025-4

Herbert, T. D., Lawrence, K. T., Tzanova, A., Peterson, L. C., Caballero-Gill, R., & Kelly, C. S. (2016, November). Late Miocene global cooling and the rise of modern ecosystems. *Nature Geoscience*, *9*(11), 843–847. Retrieved 2020-11-09, from http://www.nature.com/articles/ngeo2813 doi: 10.1038/ngeo2813

Hermoyian, C. S., & Owen, R. M. (2001, February). Late Miocene-early Pliocene biogenic bloom: Evidence from low-productivity regions of the Indian and Atlantic Oceans. *Paleoceanography*, *16*(1), 95–100. Retrieved 2020-11-09, from http://doi.wiley.com/10.1029/2000PA000501 doi: 10.1029/2000PA000501

Herold, N., Huber, M., Müller, R. D., & Seton, M. (2012, March). Modeling the Miocene climatic optimum: Ocean circulation: MODELING MIOCENE OCEAN CIRCULATION. *Paleoceanography*, *27*(1), n/a–n/a. Retrieved 2020-08-28, from http://doi.wiley.com/10.1029/2010PA002041 doi: 10.1029/2010PA002041

Hodell, D. A., Curtis, J. H., Sierro, F. J., & Raymo, M. E. (2001). Correlation of Late Miocene to Early Pliocene sequences between the Mediterranean and North Atlantic. *Paleoceanography*, *16*(2), 164–178. Retrieved 2022-06-30, from http://onlinelibrary.wiley.com/doi/abs/10.1029/1999PA000487 (_eprint: https://agupubs.onlinelibrary.wiley.com/doi/pdf/10.1029/1999PA000487) doi: 10.1029/1999PA000487

Hodell, D. A., & Venz-Curtis, K. A. (2006). Late Neogene history of deepwater ventilation in the Southern Ocean. *Geochemistry, Geophysics, Geosystems*, *7*(9). Retrieved 2022-07-10, from http://onlinelibrary.wiley.com/doi/abs/10.1029/2005GC001211 (_eprint: https://agupubs.onlinelibrary.wiley.com/doi/pdf/10.1029/2005GC001211) doi: 10.1029/2005GC001211

Holbourn, A. E., Kuhnt, W., Clemens, S. C., Kochhann, K. G. D., Jöhnck, J.,

Lübbers, J., & Andersen, N. (2018, December). Late Miocene climate cooling and intensification of southeast Asian winter monsoon. *Nature Communications*, *9*(1), 1584. Retrieved 2022-07-20, from http://www.nature.com/articles/s41467-018-03950-1 doi: 10.1038/s41467-018-03950-1

Hossain, A., Knorr, G., Lohmann, G., Stärz, M., & Jokat, W. (2020, July). Simulated Thermohaline Fingerprints in Response to Different Greenland-Scotland Ridge and Fram Strait Subsidence Histories. *Paleoceanography and Paleoclimatology*, *35*(7). Retrieved 2021-05-10, from https://onlinelibrary.wiley.com/doi/abs/10.1029/2019PA003842 doi: 10.1029/2019PA003842

Hovan, S. A. (1995). 28. Late Cenozoic atmospheric circulation intensity and climatic history recorded by Eolian deposition in the Eastern Equatorial Pacific Ocean, Leg 138. *Proceedings of the Ocean Drilling Program, Scientific Results. Proceedings of the Ocean Drilling Program, Scientific Results*, 615–625.

Huguet, C., Jaeschke, A., & Rethemeyer, J. (2022). Paleoclimatic and palaeoceanographic changes coupled to the Panama Isthmus closing (13–4Ma) using organic proxies. , 40.

Janecek, T. R. (1985, November). Eolian sedimentation in the northwest pacific ocean: A preliminary examination of the data from deep sea drilling project sites 576 and 578. , *86*. Retrieved 2022-03-15, from http://deepseadrilling.org/86/dsdp_toc.htm doi: 10.2973/dsdp.proc.86.1985

John, S., & Krissek, L. A. (2002). The late Miocene to Pleistocene ice-rafting history of southeast Greenland. , 8.

Kamae, Y., Ueda, H., & Kitoh, A. (2011). Hadley and Walker Circulations in the Mid-Pliocene Warm Period Simulated by an Atmospheric General Circulation Model. *Journal of the Meteorological Society of Japan. Ser. II*, *89*(5), 475–493. Retrieved 2022-09-26, from http://www.jstage.jst.go.jp/article/jmsj/89/5/89_5_475/_article doi: 10.2151/jmsj.2011-505

Karatsolis, B. ., Lougheed, B. C., De Vleeschouwer, D., & Henderiks, J. (2022, December). Abrupt conclusion of the late Miocene-early Pliocene biogenic bloom at 4.6-4.4 Ma. *Nature Communications*, *13*(1), 353. Retrieved 2022-01-25, from https://www.nature.com/articles/s41467-021-27784-6 doi: 10.1038/s41467-021-27784-6

Keigwin, L. D. (1979). LATE CENOZOIC STABLE ISOTOPE STRATIGRAPHY AND PALEOCEANOGRAPHY OF DSDP SITES FROM THE EAST EQUATORIAL AND CENTRAL NORTH PACIFIC OCEAN. , 22.

Kuhnt, W., Holbourn, A., Hall, R., Zuvela, M., & Käse, R. (2004). Neogene History of the Indonesian Throughflow. In *Continent-Ocean Interactions Within East Asian Marginal Seas* (pp. 299–320). American Geophysical Union (AGU). Retrieved 2022-09-22, from http://onlinelibrary.wiley.com/doi/abs/10.1029/149GM16 (_eprint: https://agupubs.onlinelibrary.wiley.com/doi/pdf/10.1029/149GM16) doi: 10.1029/149GM16

Lyle, M. (2003). Neogene carbonate burial in the Pacific Ocean. *Paleoceanography*, *18*(3). Retrieved 2022-03-15, from http://onlinelibrary.wiley.com/doi/abs/10.1029/2002PA000777 (_eprint: https://agupubs.onlinelibrary.wiley.com/doi/pdf/10.1029/2002PA000777) doi: 10.1029/2002PA000777

Lyle, M., & Baldauf, J. (2015, September). Biogenic sediment regimes in the Neogene equatorial Pacific, IODP Site U1338: Burial, production, and diatom community. *Palaeogeography, Palaeoclimatology, Palaeoecology*, *433*, 106–128. Retrieved 2020-11-09, from https://linkinghub.elsevier.com/retrieve/pii/S0031018215001868 doi: 10.1016/j.palaeo.2015.04.001

Lyle, M., Dadey, K. A., & Farrel, J. W. (1995, August). The late miocene (11-8 ma) eastern pacific carbonate crash: Evidence for reorganization of deep-water circulation by the closure of the panama gateway. , *138*. Retrieved 2022-10-04,

from http://www-odp.tamu.edu/publications/138_SR/138TOC.HTM doi: 10.2973/odp.proc.sr.138.1995

Lyle, M., Drury, A. J., Tian, J., Wilkens, R., & Westerhold, T. (2019, September). Late Miocene to Holocene high-resolution eastern equatorial Pacific carbonate records: stratigraphy linked by dissolution and paleoproductivity. *Climate of the Past*, *15*(5), 1715–1739. Retrieved 2022-03-15, from https://cp.copernicus.org/articles/15/1715/2019/ doi: 10.5194/cp-15-1715-2019

Lübbers, J., Kuhnt, W., Holbourn, A., Bolton, C., Gray, E., Usui, Y., ... Andersen, N. (2019, May). The Middle to Late Miocene "Carbonate Crash" in the Equatorial Indian Ocean. *Paleoceanography and Paleoclimatology*, *34*(5), 813–832. Retrieved 2022-09-19, from https://hal.archives-ouvertes.fr/hal-02341889 (Publisher: American Geophysical Union) doi: 10.1029/2018PA003482

Martinot, C., Bolton, C. T., Sarr, A.-C., Donnadieu, Y., Garcia, M., Gray, E., & Tachikawa, K. (2022). *Drivers of late Miocene tropical sea surface cooling: a new perspective from the equatorial Indian Ocean* (accepted). Environmental Sciences. Retrieved 2022-07-05, from http://www.essoar.org/doi/10.1002/essoar.10509655.2 doi: 10.1002/essoar.10509655.2

Montes, C., Cardona, A., Jaramillo, C., Pardo, A., Silva, J. C., Valencia, V., ... Nino, H. (2015, April). Middle Miocene closure of the Central American Seaway. *Science*, *348*(6231), 226–229. Retrieved 2021-05-10, from https://www.sciencemag.org/lookup/doi/10.1126/science.aaa2815 doi: 10.1126/science.aaa2815

Müller, D. W., Hodell, D. A., & Ciesielski, P. F. (1991, February). Late miocene to earliest pliocene (9.8-4.5 ma) paleoceanographyofthe subantarctic southeast atlantic: Stable isotopic, sedimentologic, and microfossil evidence. , *114*. Retrieved 2022-03-15, from http://www-odp.tamu.edu/publications/114_SR/114TOC.HTM doi: 10.2973/odp.proc.sr.114.1991

NASA Goddard Space Flight Center. (2022). Ocean ecology laboratory, ocean biology processing group. moderate-resolution imaging spectroradiometer (modis) aqua chlorophyll data; 2022 reprocessing. nasa ob.daac, greenbelt, md, usa. Retrieved from oceancolor.gsfc.nasa.gov/l3/ ([Dataset]) doi: 10.5067/AQUA/MODIS/L3B/CHL/2022.

Nisancioglu, K. H., Raymo, M. E., & Stone, P. H. (2003, March). Reorganization of Miocene deep water circulation in response to the shoaling of the Central American Seaway: REORGANIZATION OF MIOCENE DEEP WATER CIRCULATION. *Paleoceanography*, *18*(1), n/a–n/a. Retrieved 2021-05-10, from http://doi.wiley.com/10.1029/2002PA000767 doi: 10.1029/2002PA000767

O'Dea, A., Lessios, H. A., Coates, A. G., Eytan, R. I., Restrepo-Moreno, S. A., Cione, A. L., ... Jackson, J. B. C. (2016, August). Formation of the Isthmus of Panama. *Science Advances*, *2*(8), e1600883. Retrieved 2022-09-22, from https://www.science.org/doi/10.1126/sciadv.1600883 doi: 10.1126/sciadv.1600883

Palike, H., Norris, R. D., Herrle, J. O., Wilson, P. A., Coxall, H. K., Lear, C. H., ... Wade, B. S. (2006). The heartbeat of the Oligocene climate system. *science*, *314*(5807), 1894–1898. (Publisher: American Association for the Advancement of Science)

Peterson, L., & Backman, J. (1990). Late cenozoic carbonate accumulation and the history of the carbonate compensation depth in the western equatorial indian ocean. , 467–507.

Pillot, Q., Donnadieu, Y., Sarr, A.-C., Ladant, J.-B., & Suchéras-Marx, B. (2022). Evolution of Ocean Circulation in the North Atlantic Ocean During the Miocene: Impact of the Greenland Ice Sheet and

the Eastern Tethys Seaway. *Paleoceanography and Paleoclimatology*, *37*(8), e2022PA004415. Retrieved 2022-09-07, from http://onlinelibrary.wiley.com/doi/abs/10.1029/2022PA004415 (_eprint: https://agupubs.onlinelibrary.wiley.com/doi/pdf/10.1029/2022PA004415) doi: 10.1029/2022PA004415

Pisias, N., Mayer, L., Janecek, T., Palmer-Julson, A., & van Andel, T. (Eds.). (1995). *Proceedings of the Ocean Drilling Program, 138 Scientific Results* (Vol. 138). Ocean Drilling Program. Retrieved 2020-12-15, from http://www-odp.tamu.edu/publications/138_SR/138TOC.HTM doi: 10.2973/odp.proc.sr.138.1995

Poore, H. R., Samworth, R., White, N. J., Jones, S. M., & McCave, I. N. (2006, June). Neogene overflow of Northern Component Water at the Greenland-Scotland Ridge: NEOGENE OVERFLOW OF NCW. *Geochemistry, Geophysics, Geosystems*, *7*(6), n/a–n/a. Retrieved 2021-06-11, from http://doi.wiley.com/10.1029/2005GC001085 doi: 10.1029/2005GC001085

Pound, M. J., Haywood, A. M., Salzmann, U., & Riding, J. B. (2012, April). Global vegetation dynamics and latitudinal temperature gradients during the Mid to Late Miocene (15.97–5.33Ma). *Earth-Science Reviews*, *112*(1-2), 1–22. Retrieved 2022-07-04, from https://linkinghub.elsevier.com/retrieve/pii/S0012825212000165 doi: 10.1016/j.earscirev.2012.02.005

Pälike, H., Lyle, M. W., Nishi, H., Raffi, I., Ridgwell, A., Gamage, K., ... Zeebe, R. E. (2012, August). A Cenozoic record of the equatorial Pacific carbonate compensation depth. *Nature*, *488*(7413), 609–614. Retrieved 2022-03-15, from http://www.nature.com/articles/nature11360 doi: 10.1038/nature11360

Qin, X., Müller, R. D., Cannon, J., Landgrebe, T. C. W., Heine, C., Watson, R. J., & Turner, M. (2012, October). The GPlates Geological Information Model and Markup Language. *Geoscientific Instrumentation, Methods and Data Systems*, *1*(2), 111–134. Retrieved 2022-09-22, from https://gi.copernicus.org/articles/1/111/2012/ doi: 10.5194/gi-1-111-2012

Rae, J. W., Zhang, Y. G., Liu, X., Foster, G. L., Stoll, H. M., & Whiteford, R. D. (2021, May). Atmospheric CO $_2$ over the Past 66 Million Years from Marine Archives. *Annual Review of Earth and Planetary Sciences*, *49*(1), 609–641. Retrieved 2021-09-01, from https://www.annualreviews.org/doi/10.1146/annurev-earth-082420-063026 doi: 10.1146/annurev-earth-082420-063026

Reghellin, D., Coxall, H. K., Dickens, G. R., Galeotti, S., & Backman, J. (2022). The Late Miocene-Early Pliocene Biogenic Bloom in the Eastern Equatorial Pacific: New Insights From Integrated Ocean Drilling Program Site U1335. *Paleoceanography and Paleoclimatology*, *37*(3), e2021PA004313. Retrieved 2022-03-01, from http://onlinelibrary.wiley.com/doi/abs/10.1029/2021PA004313 (_eprint: https://agupubs.onlinelibrary.wiley.com/doi/pdf/10.1029/2021PA004313) doi: 10.1029/2021PA004313

Renaudie, J., Lazarus, D., & Diver, P. (2020). NSB (Neptune Sandbox Berlin): An expanded and improved database of marine planktonic microfossil data and deep-sea stratigraphy. *Palaeontologia Electronica*. Retrieved 2022-03-15, from https://palaeo-electronica.org/content/2020/2966-the-nsb-database doi: 10.26879/1032

Sarr, A.-C., Donnadieu, Y., Bolton, C. T., Ladant, J.-B., Licht, A., Fluteau, F., ... Dupont-Nivet, G. (2022, April). Neogene South Asian monsoon rainfall and wind histories diverged due to topographic effects. *Nature Geoscience*, *15*(4), 314–319. Retrieved 2022-06-22, from https://www.nature.com/articles/s41561-022-00919-0 doi: 10.1038/s41561-022-00919-0

Schneider, B., & Schmittner, A. (2006, June). Simulating the impact of the Panamanian seaway closure on ocean circulation, marine productivity and nutrient cycling. *Earth and Planetary Science Letters*, *246*(3-4), 367–380. Re-

trieved 2021-10-28, from https://linkinghub.elsevier.com/retrieve/pii/S0012821X0600330X doi: 10.1016/j.epsl.2006.04.028

Schuster, M., Duringer, P., Ghienne, J.-F., Vignaud, P., Mackaye, H. T., Likius, A., & Brunet, M. (2006, February). The Age of the Sahara Desert. *Science*, *311*(5762), 821–821. Retrieved 2022-07-19, from https://www.science.org/doi/10.1126/science.1120161 doi: 10.1126/science.1120161

Scotese, C. (2016). PALEOMAP PaleoAtlas for GPlates and the PaleoData plotter program. *PALEOMAP project*.

Sepulchre, P., Arsouze, T., Donnadieu, Y., Dutay, J.-C., Jaramillo, C., Le Bras, J., ... Waite, A. J. (2014, March). Consequences of shoaling of the Central American Seaway determined from modeling Nd isotopes. *Paleoceanography*, *29*(3), 176–189. Retrieved 2021-05-10, from http://doi.wiley.com/10.1002/2013PA002501 doi: 10.1002/2013PA002501

Sepulchre, P., Caubel, A., Ladant, J.-B., Bopp, L., Boucher, O., Braconnot, P., ... Tardif, D. (2020, July). IPSL-CM5A2 – an Earth system model designed for multi-millennial climate simulations. *Geoscientific Model Development*, *13*(7), 3011–3053. Retrieved 2022-01-03, from https://gmd.copernicus.org/articles/13/3011/2020/ doi: 10.5194/gmd-13-3011-2020

Shankle, M. G., Burls, N. J., Fedorov, A. V., Thomas, M. D., Liu, W., Penman, D. E., ... Hull, P. M. (2021, October). Pliocene decoupling of equatorial Pacific temperature and pH gradients. *Nature*, *598*(7881), 457–461. Retrieved 2022-07-05, from https://www.nature.com/articles/s41586-021-03884-7 doi: 10.1038/s41586-021-03884-7

Si, W., & Rosenthal, Y. (2019, October). Reduced continental weathering and marine calcification linked to late Neogene decline in atmospheric CO2. *Nature Geoscience*, *12*(10), 833–838. Retrieved 2021-02-03, from http://www.nature.com/articles/s41561-019-0450-3 doi: 10.1038/s41561-019-0450-3

Stax, R., & Stein, R. (1993, April). LONG-TERM CHANGES IN THE ACCUMULATION OF ORGANIC CARBON IN NEOGENE SEDIMENTS, ONTONG JAVA PLATEAU. , *130*. Retrieved 2022-03-15, from http://www-odp.tamu.edu/publications/130_SR/130TOC.HTM doi: 10.2973/odp.proc.sr.130.1993

Steinthorsdottir, M., Coxall, H. K., de Boer, A. M., Huber, M., Barbolini, N., Bradshaw, C. D., ... Strömberg, C. A. E. (2021, April). The Miocene: The Future of the Past. *Paleoceanography and Paleoclimatology*, *36*(4). Retrieved 2021-05-06, from https://onlinelibrary.wiley.com/doi/10.1029/2020PA004037 doi: 10.1029/2020PA004037

Tauxe, L., & Feakins, S. J. (2020). A Reassessment of the Chronostratigraphy of Late Miocene C3–C4 Transitions. *Paleoceanography and Paleoclimatology*, *35*(7), e2020PA003857. Retrieved 2022-07-19, from http://onlinelibrary.wiley.com/doi/abs/10.1029/2020PA003857 (_eprint: https://agupubs.onlinelibrary.wiley.com/doi/pdf/10.1029/2020PA003857) doi: 10.1029/2020PA003857

Thomas, D. J., & Via, R. K. (2007). Neogene evolution of Atlantic thermohaline circulation: Perspective from Walvis Ridge, southeastern Atlantic Ocean. *Paleoceanography*, *22*(2). Retrieved 2022-07-06, from http://onlinelibrary.wiley.com/doi/abs/10.1029/2006PA001297 (_eprint: https://agupubs.onlinelibrary.wiley.com/doi/pdf/10.1029/2006PA001297) doi: 10.1029/2006PA001297

Wagner, T. (2002, April). Late Cretaceous to early Quaternary organic sedimentation in the eastern Equatorial Atlantic. *Palaeogeography, Palaeoclimatology, Palaeoecology*, *179*(1-2), 113–147. Retrieved 2022-03-15, from https://linkinghub.elsevier.com/retrieve/pii/S0031018201004151 doi: 10.1016/S0031-0182(01)00415-1

Wang, C., Dai, J., Zhao, X., Li, Y., Graham, S. A., He, D., ... Meng, J. (2014, May). Outward-growth of the Tibetan Plateau during the Cenozoic: A review. *Tectonophysics*, *621*, 1–43. Retrieved 2022-07-06, from https://linkinghub.elsevier.com/retrieve/pii/S0040195114000729 doi: 10.1016/j.tecto.2014.01.036

Wang, R., Li, J., & Li, B. (2004). DATA REPORT: LATE MIOCENE–QUATERNARY BIOGENIC OPAL ACCUMULATION AT ODP SITE 1143, SOUTHERN SOUTH CHINA SEA. , 12.

Westerhold, T., Marwan, N., Drury, A. J., Liebrand, D., Agnini, C., Anagnostou, E., ... Zachos, J. C. (2020, September). An astronomically dated record of Earth's climate and its predictability over the last 66 million years. *Science*, *369*(6509), 1383–1387. Retrieved 2021-01-28, from https://www.sciencemag.org/lookup/doi/10.1126/science.aba6853 doi: 10.1126/science.aba6853

Winkler, A. (1999). GEOMAR Forschungszentrum fÃ¼r marine Geowissenschaften WischhofstraÃŸ 1-3, 24148 Kiel, Bundesrepublik Deutschland. , 130.

Wright, J. D., & Miller, K. G. (1996). Control of North Atlantic Deep Water Circulation by the Greenland-Scotland Ridge. *Paleoceanography*, *11*(2), 157–170. Retrieved 2022-07-06, from http://onlinelibrary.wiley.com/doi/abs/10.1029/95PA03696 (_eprint: https://agupubs.onlinelibrary.wiley.com/doi/pdf/10.1029/95PA03696) doi: 10.1029/95PA03696

Yang, R., Yang, Y., Fang, X., Ruan, X., Galy, A., Ye, C., ... Han, W. (2019). Late Miocene Intensified Tectonic Uplift and Climatic Aridification on the Northeastern Tibetan Plateau: Evidence From Clay Mineralogical and Geochemical Records in the Xining Basin. *Geochemistry, Geophysics, Geosystems*, *20*(2), 829–851. Retrieved 2022-07-20, from http://onlinelibrary.wiley.com/doi/abs/10.1029/2018GC007917 (_eprint: https://agupubs.onlinelibrary.wiley.com/doi/pdf/10.1029/2018GC007917) doi: 10.1029/2018GC007917

Zhang, L., Chen, M., Xiang, R., Zhang, L., & Lu, J. (2009, June). Productivity and continental denudation history from the South China Sea since the late Miocene. *Marine Micropaleontology*, *72*(1-2), 76–85. Retrieved 2020-11-09, from https://linkinghub.elsevier.com/retrieve/pii/S0377839809000383 doi: 10.1016/j.marmicro.2009.03.006

Zhang, Y. G., Pagani, M., Henderiks, J., & Ren, H. (2017, June). A long history of equatorial deep-water upwelling in the Pacific Ocean. *Earth and Planetary Science Letters*, *467*, 1–9. Retrieved 2022-07-05, from https://linkinghub.elsevier.com/retrieve/pii/S0012821X17301462 doi: 10.1016/j.epsl.2017.03.016

Zhang, Z., Ramstein, G., Schuster, M., Li, C., Contoux, C., & Yan, Q. (2014, September). Aridification of the Sahara desert caused by Tethys Sea shrinkage during the Late Miocene. *Nature*, *513*(7518), 401–404. Retrieved 2022-09-22, from http://www.nature.com/articles/nature13705 doi: 10.1038/nature13705